Talanta 134 (2015) 514–523

Contents lists available at ScienceDirect

Talanta

journal homepage: www.elsevier.com/locate/talanta

Fourier transform spectral imaging microscopy (FT-SIM) and scanning Raman microscopy for the detection of indoor common contaminants on the surface of dental implants

Anna Lutin [a], Valery Bulatov [a], Yusuf Jadwat [b], Neil H. Wood [b], Liviu Feller [b], Israel Schechter [a,*]

[a] Schulich department of chemistry, Technion – Israel Institute of Technology, Haifa 32000, Israel
[b] Periodontology and Oral Medicine, School of Oral Health Sciences, Faculty of Health Sciences, University of Limpopo, Medunsa Campus, 0204, South Africa

ARTICLE INFO

Article history:
Received 14 October 2014
Received in revised form
22 November 2014
Accepted 24 November 2014
Available online 2 December 2014

Keywords:
Dental
Inplant
Contamination
Spectroscopy
Analysis

ABSTRACT

Endosteal dental implants are used routinely with high success rates to rehabilitate the integrity of the dentition. However if implant surfaces become contaminated by foreign material, osseointegration may not occur and the dental implant will fail because of the lack of mechanical stability. Detection and characterization of dental implant surface contaminants is a difficult task. In this article we investigate the application of several spectral microscopy methods to detect airborne contaminants on dental implant surfaces. We found that Fourier Transform Spectral Imaging Microscopy (FT-SIM) and scanning Raman microscopy provided the most useful information. Some implants possess weak and homogeneous auto-fluorescence and are best analyzed using FT-SIM methods, while others are Raman inactive and can be analyzed using scanning Raman microscopy.

1. Introduction

Endosseous osseointegrated dental implants are used routinely in dentistry and generally have a long-term success rate [1,2], providing functional and aesthetically pleasing implant-borne dental restorations [3]. Osseointegration can be defined as a healing process of bone around implants, the outcome of which is the establishment and maintenance of a clinically asymptomatic rigid fixation of an alloplastic material in bone under functional loading [4]. However, uncommonly implants fail to osseointegrate because of a variety of causes including contamination of the implant surface by foreign material [5]. These contaminants may affect cellular responses in the peri-implant microenvironment immediately after implant placement, resulting in fibrous encapsulation of the implant without adequate mechanical stability [6].

Most dental implant surgical procedures are carried out in dental surgeries, in which the air is neither filtered nor pre-treated. Under such conditions it is reasonable to assume that the concentration of airborne particulates is similar to that found in other rooms in the same area. The indoor concentration of airborne particulates in common residential areas strongly depends on the outdoor conditions [7] and is of the order of 10^2–10^4 particles per cubic centimeter. The airborne particles are usually classified by their size, and about 40% of them are coarse particles (1–10 μm) and about 60% are fine particles (0.1–1 μm). The ultrafine particles (<100 nm) are difficult to monitor but their concentration is probably higher. The chemical composition of the indoor airborne particles is affected by the local outdoor environment, and it includes inorganic compounds (such as salts, oxides and calcium carbonate), biological species (such as spores, pollens and viruses) and organic matter (such as soot and polycyclic aromatic hydrocarbons). The concentration of bioaerosols is of the order of a few thousands of particles per cubic meter. [8–10]

Detection of particulate contamination on surfaces is a challenging task. [11–14] Usually, optical analysis methods are preferred because they provide fast and reliable results [11]. Several techniques have been developed and validated for analysis of aerosols adhered to surfaces, including fluorescence [14,15] and multi-photon ionization [16]. When surface imaging is of interest, Fourier Transform Spectral Imaging Microscopy (FT-SIM) [17–24] and Raman spectroscopies are known to provide detailed chemical information [25,26]. Some of these methods have the capacity to provide important information about characteristics of oral hard and soft tissues [27–30]. These methods can be applied to a large variety of materials; however, they are especially suitable to investigate contaminants of organic nature because they have

* Corresponding author. Tel./fax: +97248292579.
E-mail address: Israel@technunix.technion.ac.il (I. Schechter).

http://dx.doi.org/10.1016/j.talanta.2014.11.060
0039-9140/

the capacity to detect chemical modifications of the contaminants. [31,32]

2. Instrumental and methodological section

2.1. Instrumental

Several spectroscopic instrumental setups have been tested in this research for analysis of particulate contamination on dental implants:

1. FT-IR microscopy system, (Nicolet™ iS™5 FT-IR Spectrometer, Thermo Scientific, USA), coupled to Nicolet™ iN™10 Infrared Microscope and equipped with micro-ATR sampling device. It covers the spectral range of 7600–450 cm^{-1} at a resolution of 0.4 cm^{-1}.
2. Luminescence spectrometer (AMINCO-Bowman Series 2, Thermo Scientific, USA) equipped with two monochromators and with a front surface accessory for inspecting small surfaces. The excitation was performed using a Xenon flash lamp, in the wavelength range of 200–600 nm, and the emission was measured in the range 220–850 nm.
3. The following two systems were found to be the best suited to analyze contaminations on dental implant surfaces and provided the best performance for this application:
4. Raman microscopy system (Renishaw, 2000, U.K.). The experimental setup used for Raman spectral imaging of dental implants is depicted in Fig. 1**a**. It consists of a Raman spectrometer from Renishaw, coupled to a scientific imaging microscope (Leica DM-LM) and a high sensitivity and low noise Charge Coupled Device (CCD) detector. The latter was thermo-electrically cooled to −70 °C, reaching noise level of 7 e^{-1}pixel^{-1} and dark current of 0.0005 e^{-1} pixel^{-1} s^{-1}. The microscope was equipped with several objectives (all figures presented here were obtained using the x20 objective). The implants were manipulated using a piezoelectric stage (RGH22) of 0.1 μm resolution. For imaging purposes, a circular area on the sample was illuminated and a tunable filter was used to image the light from a selected Raman band directly onto the detector in a single step. Detailed Raman spectra at points of interest were acquired afterward, using a grating spectrometer. Excitation was performed by an air-cooled HeNe laser, emitting at 632.8 nm in a single mode (TEM000, vertically polarized). The output power was 17 mW. An air-cooled diode laser, emitting 17 mW output at 785 nm, with true single-mode operation and a line width of 0.1 cm^{-1} was also applied.
5. FT-SIM system (Green Vision, Israel). The experimental setup is described in Fig. 1**b**. A UV fluorescence microscope was coupled to a spectral imaging unit and a CCD camera. The microscope (Axiolab AB0100W/2, Carl Zeiss, Germany) was equipped with UV transparent objectives (Zeiss Fluar and Ultrafluar) providing several magnifications (x10, x20 and x40). Samples were irradiated by a mercury lamp, through the microscope objectives. Fluorescence was excited at 365 nm using a narrow band filter (10 nm). A dichroic mirror placed in the optical path was used for cutting off the reflected light at wavelengths below 390 nm. Microscope images were transferred to an imaging Fourier transform spectrometer and to a CCD camera for simultaneously recording the fluorescence spectra at each image pixel. The electro-thermally cooled CCD detector consisted of 480 × 640 pixels of 10 × 10 μm^2 each. (Hamamatsu, 4880).

2.2. Methodology

There are many potential methods that have the capacity to detect particulate contaminants on implant surfaces. The most relevant are the optical technologies, which allow for direct inspection without any pre-treatment. Obviously, in view of the size of the relevant contaminants, microscopy methods are needed. However, not all microscopic surface analysis methods are applicable to implants, because of their morphological structure. They are spirally shaped and possess large sprockets that prevent scanning and make focusing difficult.

Optical microscopy is available almost in every laboratory, however it only provides structural data, and the lack of spectral information does not allow for insight into the chemical nature of the contaminants. Therefore, microscopes equipped with fluorescence, Raman and IR spectrometers are the best candidates for inspecting dental implant surfaces. Instrumental setups that allow for surface imaging with spectral resolution in each image pixel are available. The capacity of these instruments to detect and identify particulates on dental implant surfaces were tested in this study. The results obtained using FT-IR microscopy, in the range 450–7500 cm^{-1}, were poor compared to other methods, so in the following we only report on fluorescence and Raman microscopies.

Dental implants differ in their surface properties, morphological characteristics, chemical composition and in surface treatments.

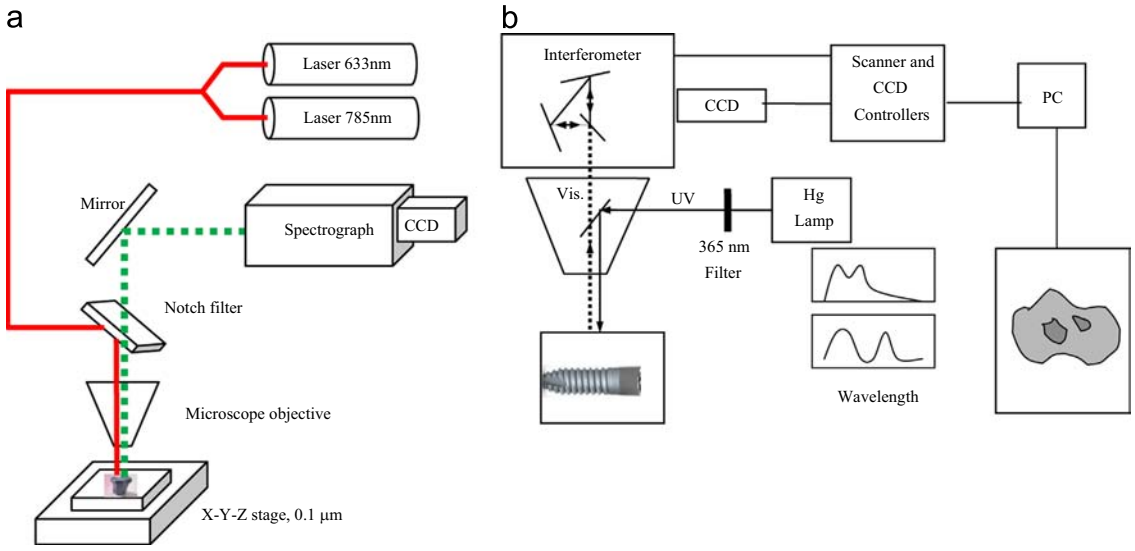

Fig. 1. The experimental setups of micro Raman (a-left) and FT-SIM imaging (b-right) used for inspecting dental implants.

The exact information on the implant surface and its manufacturing procedures are industrial secrets and are therefore not available. However, for the purpose of this study we can classify them into two groups: implants that possess weak and homogeneous fluorescence (Group A) and those which possess inhomogeneous fluorescence (Group B). The implants in group A exhibited a certain level of homogeneous auto-fluorescence, which is probably attributed to their surface nanostructure [33,34]. However, this fluorescence is weak and can be easily distinguished from that of contaminants. Group B implants also possesses weak auto-fluorescence as group A, however, the intact surfaces show spots of intensive fluorescence. These are probably attributed to surface doping or other final surface treatments. Therefore, fluorescence analysis of contaminants in group B implants is more difficult. The group B implants are Raman inactive, which allows for Raman analysis of their surfaces.

The experiments were carried out in two stages. First we exposed implants to regular room contaminants in order to find out if contaminants naturally stick to the implant surfaces and if the contaminants can be detected using FT-SIM, Raman and FT-IR facilities. In the first stage of the experiment we did not know the nature of the particulate contaminants. In the second stage we exposed the implant surfaces to known contaminants, in order to find out if they can be detected and identified on the implant surface, based on their spectral features.

3. Results and discussion

We shall now address the detection of particulates on the two main implant groups.

3.1. Group A – homogeneous implants

The majority of implants in this group possesses weak homogeneous auto-fluorescence. Microscopic fluorescence and Raman analysis of uncontaminated implants, of implants exposed to ambient room conditions and of implants which surfaces were artificially contaminated are presented in the following.

3.1.1. FT-SIM analysis

FT-SIM facility irradiates the implant with UV light and provides a microscopic fluorescence image of the inspected object. A series of interferometric images is measured and analyzed such that the spectrum of the fluorescence emission can be calculated at each pixel of the original image.

3.1.1.1. FT-SIM analysis of a group A dental implant exposed to room environment. An implant was exposed to normal room environment for 24 h. There is a certain probability that implant surfaces get contaminated even in the short period between opening their container and implant insertion into the osteotomy site. The rather long exposure used here was to ensure that a large representative sample of contaminants adhered to the implant surface.

In Fig. 2**a** we show the fluorescence imaging obtained from a random location on the implant surface. The weak background is attributed to the implant's auto-fluorescence, while the bright features are owing to contaminants. FT-SIM facility also allows for measuring the fluorescence spectra at each pixel of the image. The spectra obtained at three locations are shown in Fig. 2**b**. Location "B" represents the uncontaminated implant surface. The fluorescence at this location is weak and possesses a wide peak with a maximum at 520 nm. The spectrum of one of the contaminants is represented by location "A". The fluorescence spectrum of this contaminant is more intensive than that of the implant and has a maximum at 575 nm. Another contaminant was observed at the upper right corner of the image and it is represented by point "C". Its spectrum is intensive and its maximum is at 480 nm.

Besides exposure to air, the implant might also be accidentally dropped and consequently contaminated. In order to simulate such an event, an implant was dropped to the floor and thereafter thoroughly washed with water (distilled and filtered through 0.2 μm mesh). Surprisingly, some contaminants adhered so strongly to the implant surface that they could not be removed. A representative fluorescence image of this contaminated implant is shown in Fig. 3**a**. The contamination is clearly observed on the background of the implant. The corresponding fluorescence spectra measured at the indicated locations are shown in Fig. 3**b**.

Dental implants are easily contaminated by particulates when exposed to room air. When dropped, extensive contamination takes place which cannot be removed. It seems that the chemical and morphological nature of the implant surface promotes the adherence of airborne particulates found in dental surgeries. Fluorescence imaging is an effective tool to detect particulate contaminants. The fluorescence spectrum, which is obtained by FT-SIM facility, provides ample information that can potentially be used for identification of the chemical nature of the contaminants.

3.1.1.2. FT-SIM analysis of a dental implant contaminated with a fabric fiber. The following outlines the controlled contamination of uncontaminated group A implants and their resultant FT-SIM analysis. We contaminated the implant surface with microscopic fabric fibers which are commonly found in dental surgeries. The

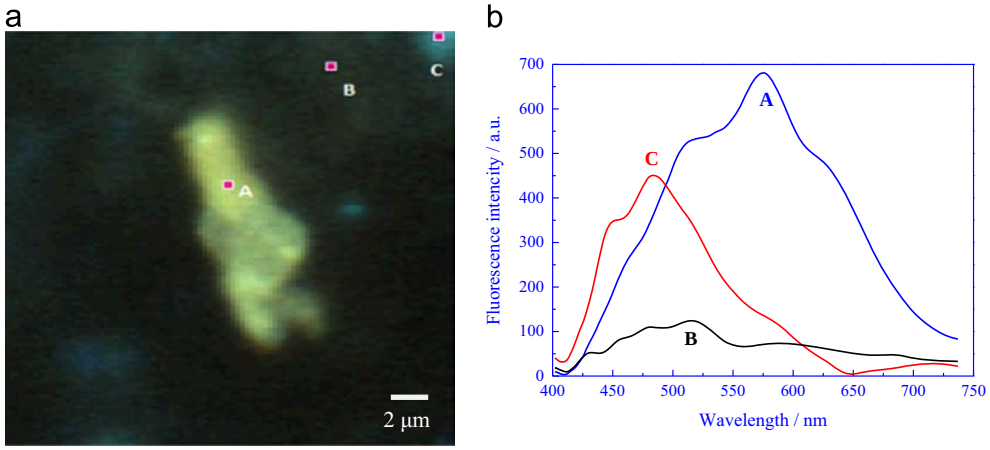

Fig. 2. (a-left) Fluorescence image of a random location on the group A implant, measured after long exposure to room air. The dark background is of the implant and the bright features show contaminants. (b-right) The fluorescence spectra of the implant and of the contaminants at the specified representative locations.

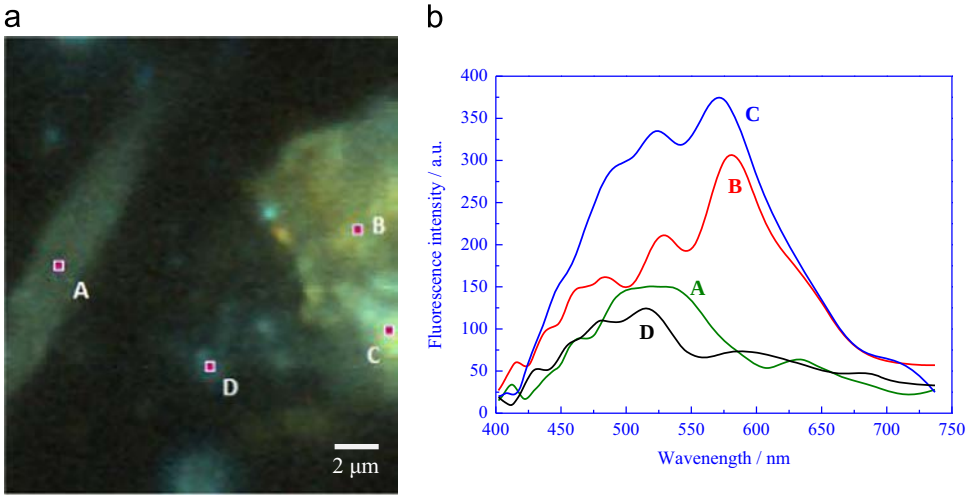

Fig. 3. (a-left) Fluorescence image of a group A implant dropped to the floor and thoroughly washed with clean water. A large variety of contaminants that could not be removed are observed. (b-right) The corresponding fluorescence spectra at the indicated locations.

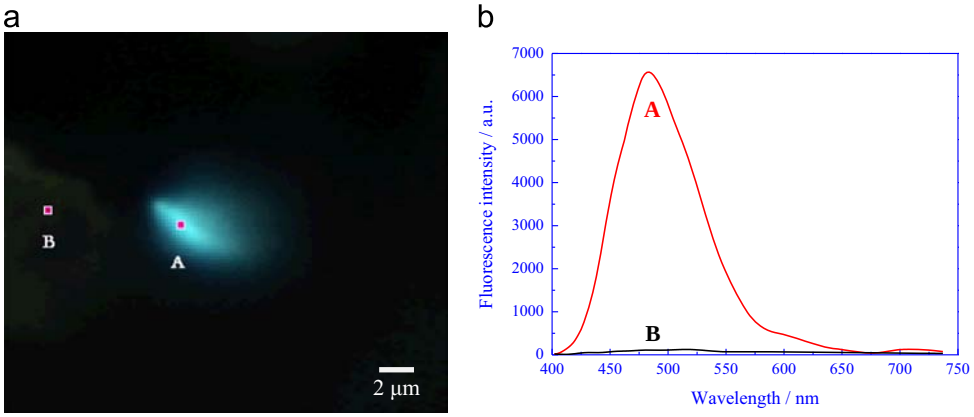

Fig. 4. (a) Microscopic fluorescence image of a group A implant contaminated with a fabric fiber. The fluorescence of the fiber is very strong and can easily be observed on the background of the implant. (b) The corresponding spectra of the fiber and of the implant are also shown. Although the wavelengths of maximum emission of the fiber and the implant are close, the substantial difference in their intensities allows for a clear detection of this contaminant.

results are shown in Fig. 4. The fiber is clearly seen on the background of the implant. The fluorescence spectrum of the fiber is very strong and has a Gaussian-like shape with a maximum at 495 nm.

3.1.1.3. FT-SIM analysis of a dental implant contaminated with pollens. Pollen concentration in air may reach high seasonal levels and they tend to adhere to surfaces. Contamination by pollens of implant surfaces might have medical consequences such as local allergic reactions. We contaminated an implant with three commonly found pollens: nerium oleander, heterotheca subaxillaris and pine.

The fluorescence image of nerium oleander pollen on an implant is shown in Fig. 5**a**. It is round with protuberances. The FT-SIM spectrum of this pollen is different than that of the implant surface in both intensity and wavelength of maximum intensity. Results of the contamination of the implant with heterotheca subaxillaris are shown in Fig. 5**b**. The shape of this pollen is different from the previous one and so is its fluorescence spectrum.

With regard to pine pollen, we could seldom observe single pine pollen contamination of the implant surface, and it seems that pine pollen tends to conglomerate. Fig. 5**c** shows characteristic pine pollen contamination on the implant. Pine pollen fluorescence is stronger than that of the implant surface and its spectrum is characteristic. However, in this case, the pollen itself has a specific structure and its fluorescence depends on location. Their fluorescence at one end is stronger than that at its surface and the spectrum obtained at that end is somewhat different. Nevertheless, their wavelength of maximum intensity is the same (525 nm).

The above experiments indicated that pollens tend to contaminate and strongly adhere to implant surfaces. The FT-SIM method can be utilized for pollen detection. Pollens can be identified by a combination of their characteristic shapes and spectral features.

3.1.1.4. FT-SIM analysis of a dental implant contaminated with PAHs.. Polycyclic aromatic hydrocarbons (PAHs) are compounds generated from incomplete combustion of organic materials such as fuel, coal, cigarettes and cooking. Numerous such emission sources are present in urban environments. The vapor pressures of most PAHs are low, so they tend to condense into airborne aerosols. Many of these particles are considered carcinogenic or mutagenic, therefore, their insertion into the body through implants should be avoided.

We tested the possibility of detecting PAH particulates on the surfaces of dental implants. PAHs possess characteristic fluorescence which can be utilized for their detection. In the following we present the results obtained from coronene particles on a group A implant.

Fig. 6 shows microscopic fluorescence image of an implant contaminated with coronene. The fluorescence intensity of coronene is so intensive that the background of the implant appears black. Clearly, the FT-SIM facility can be utilized to detect fluorescing PAHs on the surfaces of dental implants.

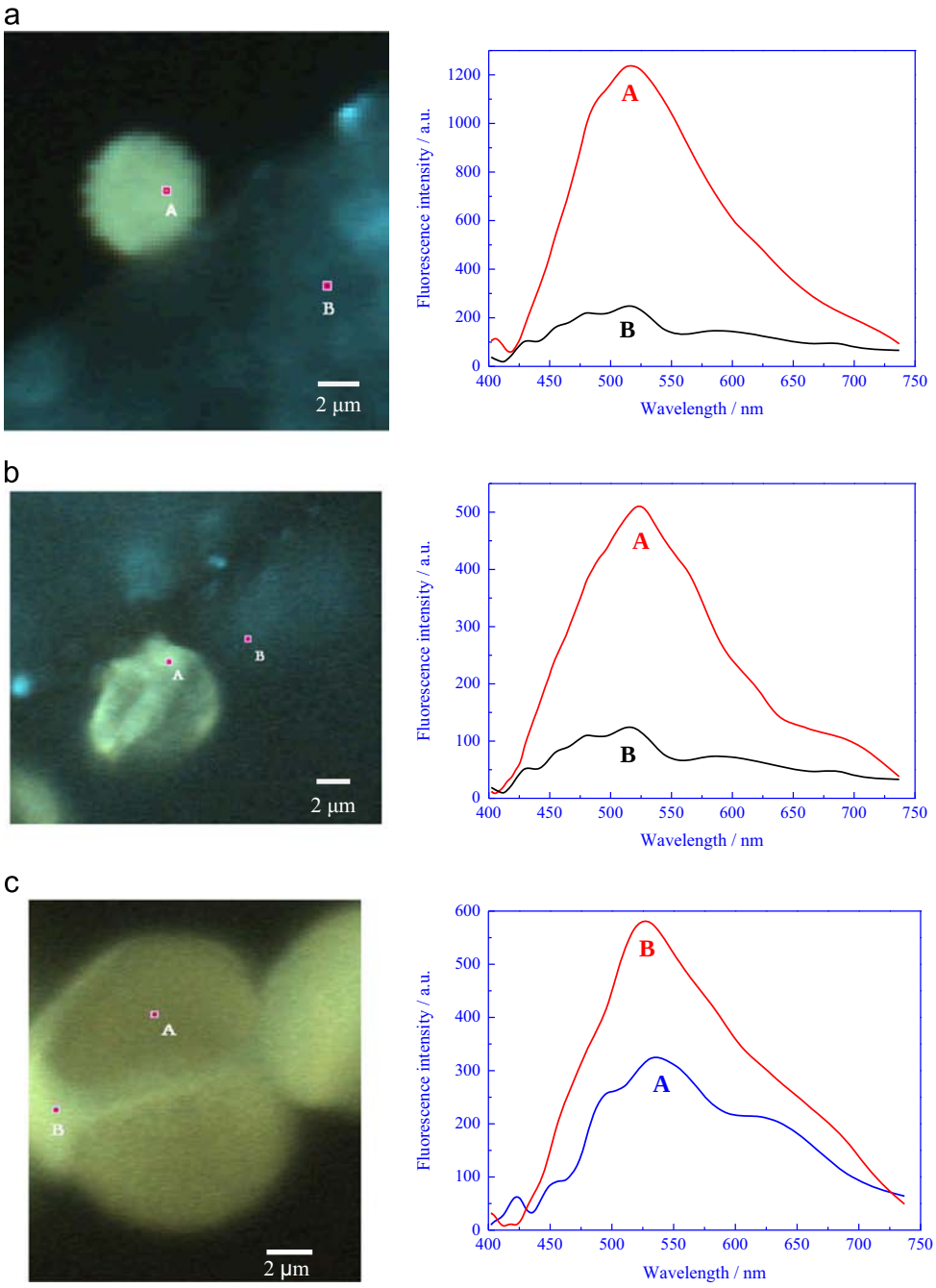

Fig. 5. Microscopic fluorescence images and spectra of the implant background and of single pollens on it. (a) Nerium oleander pollen, characterized by a round shape. The spectra of the pollen and of the implant background indicate clear distinction between them. (b) Heterotheca subaxillaris pollen. (c) A conglomerate of pine pollens on a group A implant. Their characteristic shape is clearly observed. They possess an end of higher emission intensity. The corresponding spectra of the pollen surface and of its end indicate the differences between these sites, however, the wavelength of maximum emission is the same. The pollens can clearly be observed on the implant background.

3.1.2. *Micro-Raman analysis*

Micro-Raman spectroscopy has been previously utilized for inspection of dental enamel [25,26]. Therefore it is interesting to test if this technique is adequate to detect contaminants on dental implant surfaces. Note that not all contaminants emit fluorescence and therefore the Raman method may provide important complementary information.

3.1.2.1. Raman signals of an uncontaminated group A dental implant. The major composition of dental implant surfaces is Titanium dioxide. Titanium dioxide may be found in two main polymorphs: rutile and anatase. These different crystal polymorphs possess different Raman spectra, as shown in Fig. 7. They correspond to well documented such spectra [35].

The Raman scattering of an uncontaminated group A implant and its characteristic spectrum are shown in Fig. 8. Comparison of this spectrum to those of the common polymorphs indicates that its main composition is anatase. It was probably subjected to doping and other surface processing which resulted in modification to its Raman spectrum.

3.1.2.2. Micro-Raman analysis of a group A dental implant contaminated with talc powder. Powder talc is present in the clinical environment because it is used in surgical gloves. Talc is a mineral composed

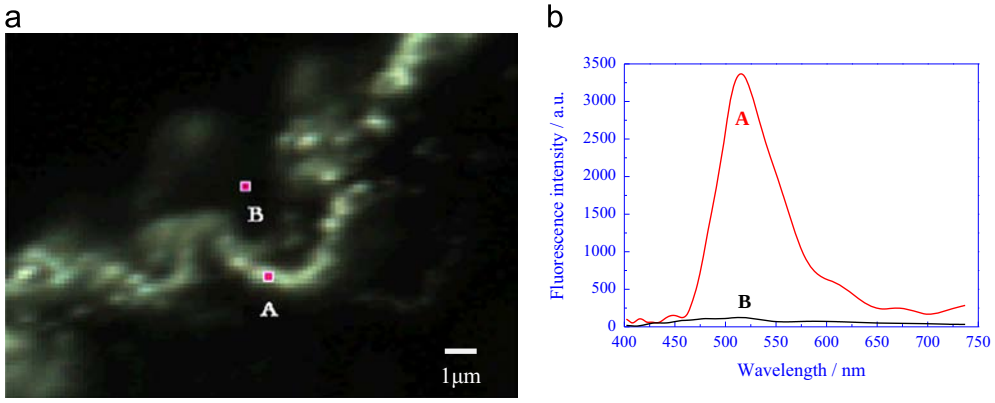

Fig. 6. (a) Microscopic fluorescence image of a coronene particle on a group A implant. Its characteristic strong emission is clearly observed. (b) The corresponding spectra of the contaminant and of the implant background indicate clear distinction between them.

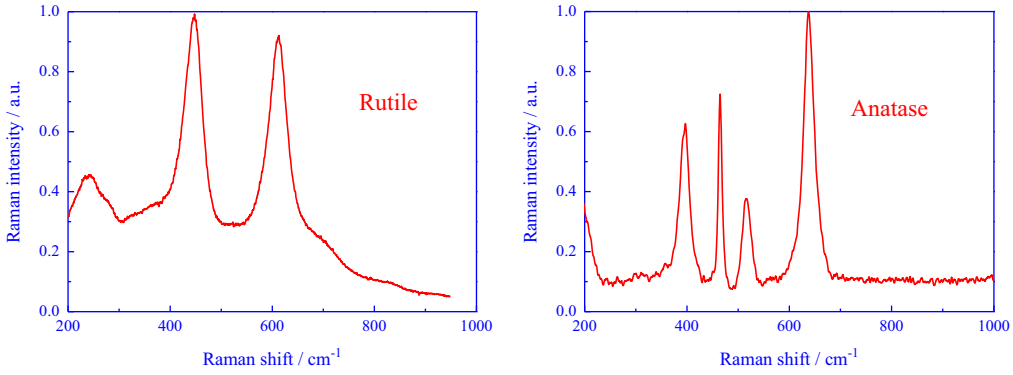

Fig. 7. Raman spectra of pure titanium dioxide polymorphs.

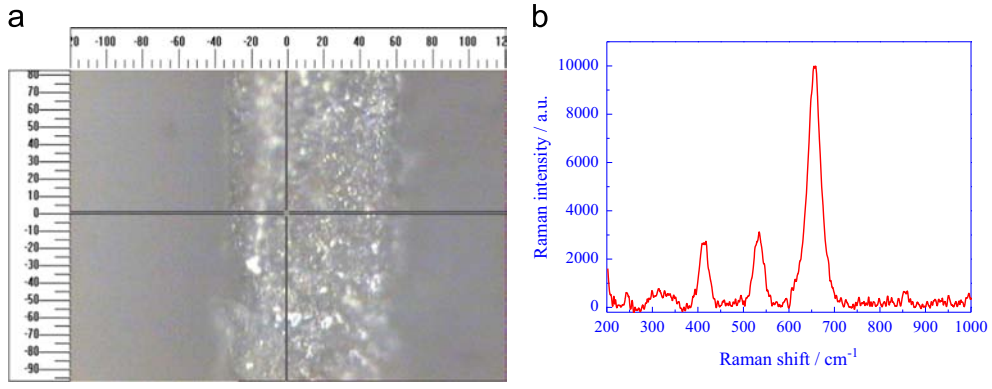

Fig. 8. (a) Microscopic image of a group A implant, taken at 20-fold enlargement (units: μm). (b) The corresponding Raman spectrum of the implant.

of hydrated magnesium silicate and it does not emit significant fluorescence. Talc tends to form conglomerates of micro-particles which may easily adhere to the implant surface.

A microscopic image of an implant contaminated with talc is shown in Fig.9**a**. The Raman spectra of the uncontaminated implant, of pure talc and of talc particles found on the implant surface are shown in Fig. 9**b**. Talc possesses three characteristic peaks at 210, 380 and 690 cm^{-1}. These peaks are different than those of the uncontaminated implant, thus allowing for detection of this contaminant. When testing the contaminated implant, the peaks of talc are clearly overlapped on the peaks of the implant. It means that micro-Raman spectroscopy can be utilized for detection of talc contamination of implants.

It has been shown that talc particles on implant surfaces have the capacity to trigger an inflammatory foreign body reaction. This results in the formation of a granuloma with the failure of the implant to osseointegrate [5].

3.1.2.3. Micro-Raman analysis of a group A dental implant contaminated with calcium carbonate. Calcium carbonate ($CaCO_3$) is a major component of the soil in many places on our planet and therefore $CaCO_3$ aerosols are very common. This compound does not emit significant fluorescence, therefore its detection based on Raman scattering is of importance.

Microscopic image of a group A implant contaminated with $CaCO_3$ is shown in Fig. 10**a**. The Raman spectra of the uncontaminated implant, of pure $CaCO_3$ and of an implant contaminated with this mineral are shown in Fig. 10**b**. Calcium carbonate possesses three characteristic peaks at 300, 725 and 1100 cm^{-1}. These peaks are much different than those of the uncontaminated implant, thus

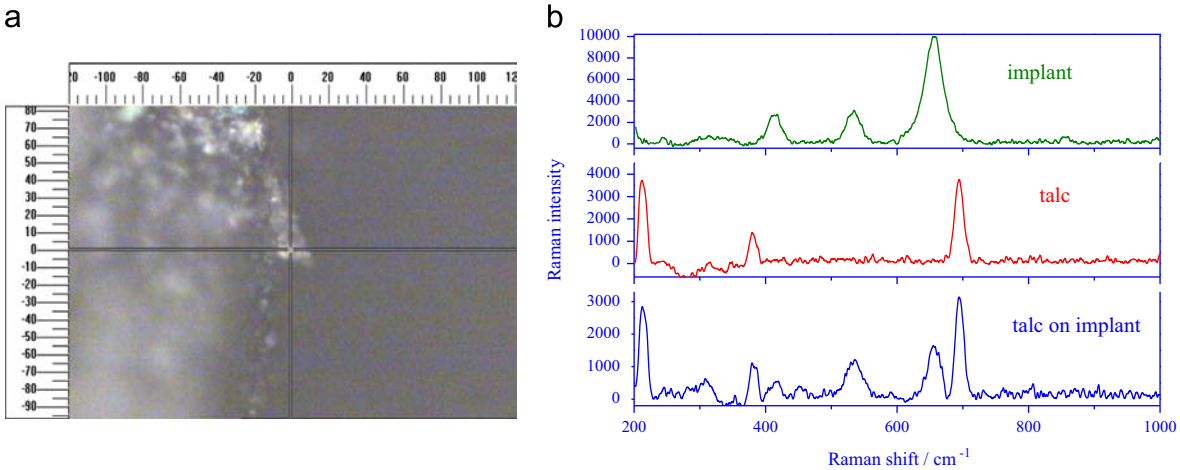

Fig. 9. (a-left) Microscopic image of a group A implant contaminated with talc (units: μm). The cross-hair indicates a contaminated spot. (b-right) The Raman spectra of the uncontaminated implant of pure talc and of the implant at a point contaminated by talc. The results indicate that the specific Raman peaks of the talc can be utilized for its detection on this implant.

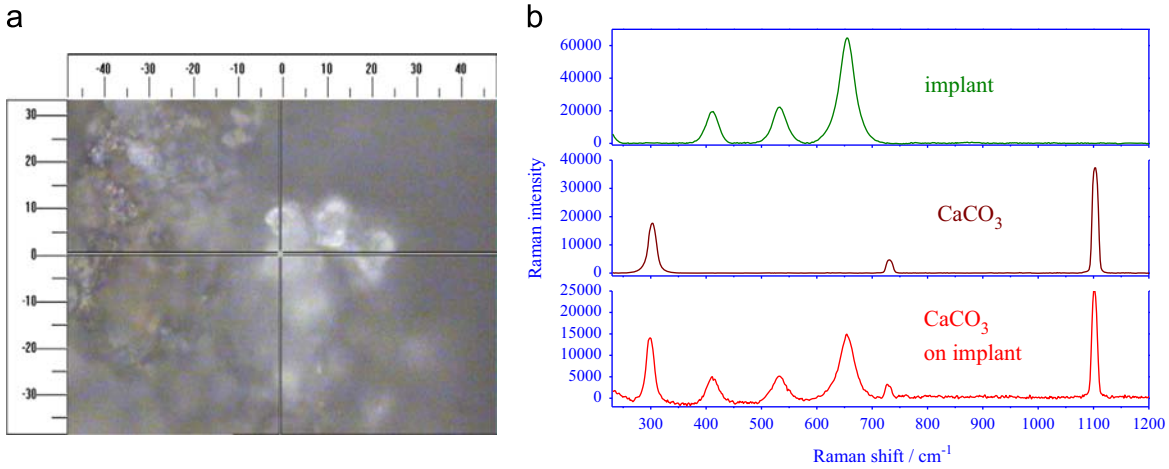

Fig. 10. (a) Microscopic image of a group A implant contaminated with calcium carbonate particulates (units: μm). The cross-hair indicates a contaminated spot. (b) The Raman spectra of the uncontaminated implant, of pure calcium carbonate and of the implant at a contaminated spot. The results indicate that the specific Raman peaks of calcium carbonate can be utilized for its detection on this implant.

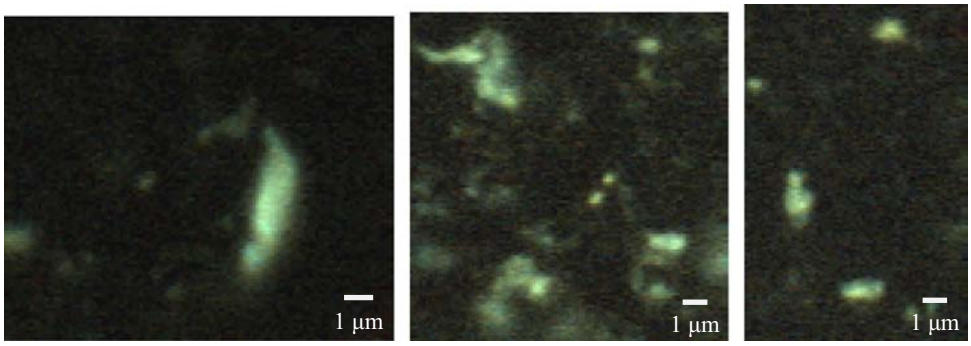

Fig. 11. Microscopic fluorescence images of a group B implant at three different locations. Measurements were performed on sterile intact implants, just after taken out of the original case.

allowing for detection of this contaminant. When testing the contaminated implant surface, the spectrum of the $CaCO_3$ and of the implant surface overlaps. This implies that micro-Raman spectroscopy can be used to detect implant contamination by $CaCO_3$.

3.2. Group B – inhomogeneous implants

As previously mentioned, some implants possess inhomogeneous auto-fluorescence. Microscopic fluorescence and Raman analysis of uncontaminated and of artificially contaminated group B implants are presented in the following.

3.2.1. FT-SIM analysis

3.2.1.1. FT-SIM analysis of uncontaminated group B dental implant. Three fluorescence microscopic images of an uncontaminated implant are shown in Fig. 11. It is clear that the surface of this implant contains many fluorescing spots that are probably attributed to the

manufacturing processes or to prior packing contaminations. We have handled the sample with much care and we believe that no considerable contamination was added during our measurements.

A large variety of fluorescing spots were observed. They differ in size, in shape and also in their characteristic spectrum. A few examples of such spots and their emission spectra are shown in

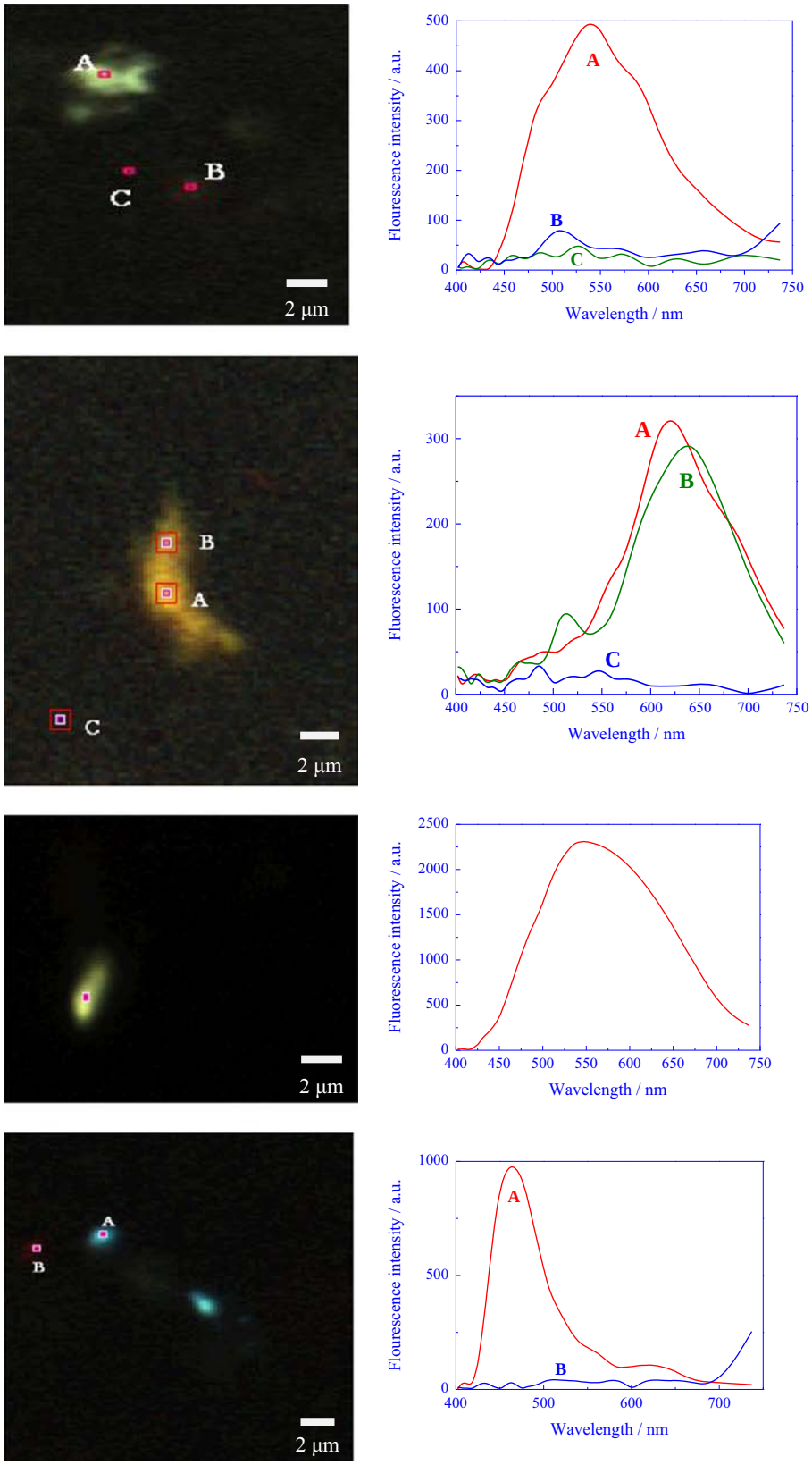

Fig. 12. Examples of microscopic fluorescence images of random locations on a group B implant and the corresponding spectra. A large variety of sizes, shapes and spectra are observed.

Fig. 12. Although the origin of these spots is unknown, it is clear that FT-SIM is not the right tool to examine implant surface contamination. Therefore, inhomogeneous implants should be tested using micro-Raman spectroscopy.

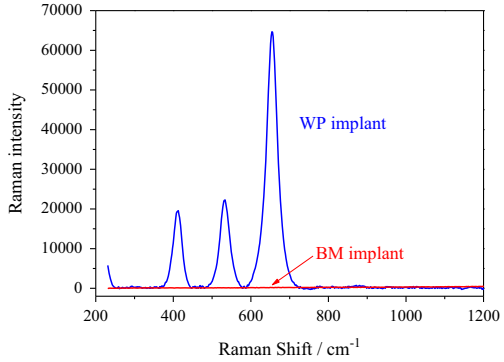

Fig. 13. Raman spectra of a group B implant compared to that of a group A implant. The scattering efficiency of the group B implant surface is much lower, which may allow for better analysis of contaminants.

3.2.2. Micro-Raman analysis

3.2.2.1. Comparison between group A and group B. The surface of an uncontaminated group B implant possesses almost no Raman scattering. Fig. 13 presents the Raman spectrum of this implant in comparison to that of a group A implant. It means that contaminants on inhomogeneous implant surfaces can easily be measured based on their Raman scattering.

3.2.2.2. Micro-Raman analysis of a group B dental implant contaminated with talc powder. The feasibility of detecting talc particulates on group B implant surfaces was tested, as done for the WP implants. The results are shown in Fig. 14. The microscopic image and the Raman spectra are shown for the uncontaminated group B implant, for the pure talc and for a contaminated spot on the implant. In this case, since the implant contribution to the Raman scattering is negligible, the spectrum of the contaminated implant is almost identical to that of the contaminant. This allows for simple and easy identification of the contaminant.

3.2.2.3. Micro-Raman analysis of a group B dental implant contaminated with calcium carbonate. As previously done with the group A implants, a group B implant was contaminated with $CaCO_3$. The results are shown in Fig. 15, where the microscopic image of the contaminated implant is presented together with the spectra of the uncontaminated implant, of

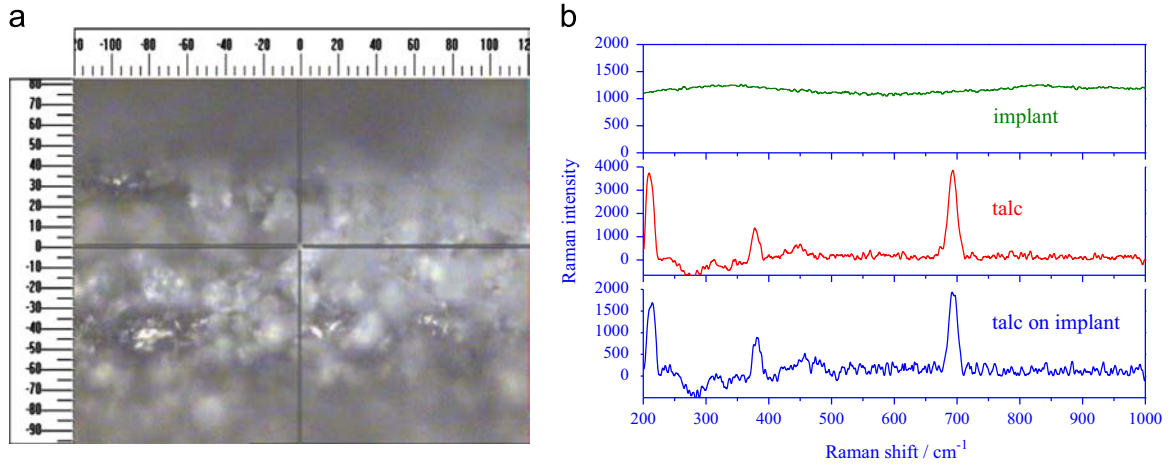

Fig. 14. (a) Microscopic image of a group B implant contaminated with talc particles (units: μm). (b) The Raman spectra of the uncontaminated implant, of pure talc and of a contaminated spot. The lack of Raman activity of the surface allows for clear identification of the contaminant.

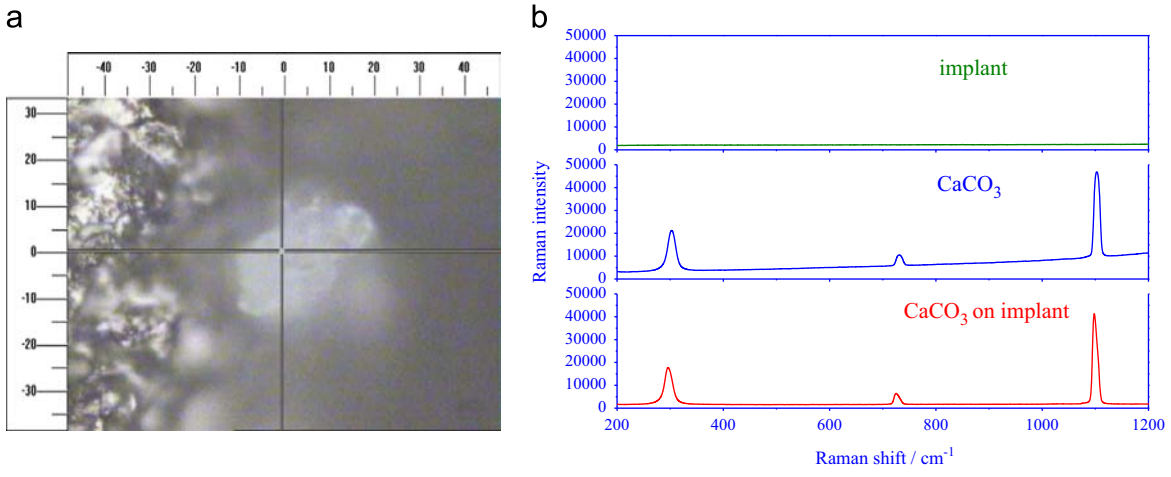

Fig. 15. (a) Microscopic image of a group B implant contaminated with calcium carbonate particles (units: μm). (b) The Raman spectra of the uncontaminated implant, of pure calcium carbonate and of a contaminated spot. The lack of Raman activity of the surface allows for clear identification of the contaminant.

pure $CaCO_3$ and of a contaminated spot. Also in this case identification of the contaminant is very clear owing to the lack of Raman activity of the implant itself.

4. Conclusions

Analysis of common airborne contaminants on dental implants can be carried out using spectral microscopy methods. However, the proper method has to be selected according to the nature of the implant surface. Implant surfaces differ in their chemical characteristics, in their morphology and in their pre-treatment, thus resulting in different spectral features. The implants that undergo weak and homogeneous auto-fluorescence are best analyzed using the FT-SIM method. Those that possess strong and inhomogeneous fluorescence are best analyzed using scanning Raman microscopy.

FR-IR microscopy was not successful for analysis of surface contaminants, however, the other studied methods provided detailed information on inorganic aerosols (e.g., talc and $CaCO_3$), organic aerosols (such as PAHs) and airborne particulates of biological nature (such as pollens). An additional interesting finding was that many aerosols strongly adhered to implant surfaces and cannot be completely removed by washing with distilled and filtered water, even under strong and prolonged sonication. This feature of the dental implant requires further investigation and will be the subject of another project.

References

[1] R.A.G. Khammissa, L. Feller, R. Meyerov, J. Lemmer, SADJ 67 (1012) 122-126.
[2] R.A.G. Khammissa, L. Feller, R. Meyerov, J. Lemmer, SADJ 67 (2012) 70–74.
[3] L. Feller, R.A.G. Khammissa, M. Bouckaert, J. Lemmer, SADJ 68 (2013) 408–410.
[4] G.A. Zarb, S. Koka, Int. J. Prosthodont. 25 (2012) 11–12.
[5] L. Feller, Y. Jadwat, R. Chandran, I. Lager, M. Altini, J. Lemmer, Implant Dentristry 23 (6) (2014) 745–752.
[6] L. Feller, R. Chandran, R.A.G. Khammissa, R. Meyerov, Y. Jadwat, M. Bouckaert, I. Schechter, J. Lemmer, SADJ 69 (2014) 110–115.
[7] I.K. Koponen, A. Asmi, P. Keronen, K. Puhto, M. Kulmala, Atmos. Environ. 35 (2001) 1465–1477.
[8] G.H. Wan, C.S. Li, Arch. Environ. Health 54 (3) (1999) 172–179.
[9] A.K.Y. Law, C.K. Chau, G.Y.S. Chan, Build. Environ. 36 (4) (2001) 527–541.
[10] J.S. Pastuszka, et al., Atmos. Environ. 34 (22) (2000) 3833–3842.
[11] M. Fisher, I. Schechter, Polynuclear aromatic hydrocarbons analysis in environmental samples, in Encyclopedia of Analytical Chemistry, in: R.A. Meyers (Ed.), John Wiley & Sons Publishers, Chichester, 2000, pp. 3143–3172.
[12] C.h. Sluszny, V.V. Gridin, V. Bulatov, I. Schechter, Rev. Anal. Chem. 21 (2) (2002) 77–165.
[13] V.V. Gridin, I. Schechter, Analysis of environmental aerosols by multiphoton ionization, Analytical Chemistry of Aerosols, in: K.R. Spurny (Ed.), CRC Press/Lewis Publishers, Boca raton, London, New York, Washington DC, 1999, pp. 215–227.
[14] S. Hassoon, I. Schechter, Anal. Chim. Acta 405 (2000) 9–15.
[15] B. Horowitz, V.V. Gridin, V. Bulatov, I. Schechter, Anal. Chem. 70 (1998) 3191–3197.
[16] V.V. Gridin, T. Inoue, T. Ogawa, I. Schechter, Instrum. Sci. Technol 28 (2000) 131–141.
[17] C.H. Sluszny, V. Bulatov, I. Schechter, Anal. Chim. Acta 367 (1998) 1–10.
[18] M. Fisher, C.H. Sluszny, B. Horowitz, V. Bulatov, V.V. Gridin, S. Hassoon, I. Schechter, Int. J. Environ. Anal. Chem. 74 (1999) 9–24.
[19] C.h. Sluszny, V.V. Gridin, V. Bulatov, I. Schechter, Rev. Anal. Chem. 19 (3-4) (2000) 303–318.
[20] C.H. Sluszny, V.V. Gridin, V. Bulatov, I. Schechter, Fresenius J. Anal. Chem. 370 (2001) 69–75.
[21] J. Levinson, C.H. Sluszny, Y. Yasman, V. Bulatov, I. Schechter, Anal. Bioanal. Chem 381 (8) (2005) 1584–1591.
[22] I. Schechter, Anal. Sci. 13 (1997) 369–372.
[23] M. Fisher, V. Bulatov, S. Hasson, I. Schechter, Anal. Chem. 70 (1998) 2409–2414.
[24] M. Fisher, V. Bulatov, I. Schechter, J. Lumin 102-103 (2003) 194–200.
[25] L. Feller, Y. Yasman, V. Bulatov, E.J. Raubenheimer, I. Schechter, Instrum. Sci. Technol 32 (2004) 467–478.
[26] V. Bulatov, L. Feller, Y. Yasman, I. Schechter, Instrum. Sci. Technol 36 (2008) 235–244.
[27] M. Fisher, L. Feller, I. Schechter, Instrum. Sci. Technol 29 (1) (2001) 11–16.
[28] M. Fisher, L. Feller, I. Schechter, Instrum. Sci. Technol 30 (2002) 225–232.
[29] L. Feller, Y. Yasman, V. Bulatov, I. Schechter, Instrum. Sci. Technol 32 (2004) 579–588.
[30] N. Vinerot, Y. Chen, V.V. Gridin, V. Bulatov, L. Feller, I. Schechter, Instrum. Sci. Technol 38 (2010) 143–150.
[31] C.H. Sluszny, V. Bulatov, V.V. Gridin, I. Schechter, Photochem. Photobiol 74 (2001) 780–786.
[32] V. Bulatov, V.V. Gridin, M. Fisher, C.H. Sluszny, I. Schechter, Israel J. Chem. 47 (2007) 195–204.
[33] M. Ben-Chorin, A. Kux, I. Schechter, Appl. Phys. Lett. 64 (1994) 481–483.
[34] I. Schechter, M. Ben-Chorin, Anal. Chem. 67 (1995) 3727–3732.
[35] O. Frank, M. Zukalova, B. Laskova, J. Kürti, J. Koltai, L. Kavan, Phys. Chem. Chem. Phys. 14 (2012) 14567–14572.